Sustainable polyethylene fabrics with engineered moisture transport for passive cooling

Sustainable polyethylene fabrics with engineered moisture transport for passive cooling

Matteo Alberghini[1,2,3], Seongdon Hong[1,4,5], L. Marcelo Lozano[1,6], Volodymyr Korolovych[1,7], Yi Huang[1], Francesco Signorato[1,2], S. Hadi Zandavi[1], Corey Fucetola[1], Ihsan Uluturk[4], Michael Y. Tolstorukov[7], Gang Chen[1], Pietro Asinari[2,8], Richard M. Osgood III[4], Matteo Fasano[2,3], and Svetlana V. Boriskina[1,*]

[1]*Massachusetts Institute of Technology, Department of Mechanical Engineering, Cambridge, MA, 02139, USA*
[2]*Department of Energy, Politecnico di Torino, Torino, Italy*
[3]*Clean Water Center, Politecnico di Torino, Torino, Italy*
[4]*U.S. Army Combat Capabilities Development Command Soldier Center, Natick, MA, USA*
[5]*Defense Agency for Technology and Quality, Seoul, Korea*
[6]*Tecnologico de Monterrey, Escuela de Ingeniería y Ciencias, Monterrey, Mexico*
[7]*Dana Farber Cancer Institute, Boston, MA, USA*
[8]*INRIM Istituto Nazionale di Ricerca Metrologica, Torino 10135, Italy*

*Corresponding author: sborisk@mit.edu , http://sboriskina.mit.edu

Abstract:

Textile industry is one of the most wasteful and polluting industries in the world. With 200 liters of water required to produce 1 kg of yarn, the industry uses over 26 trillion gallons of water annually, and pollutes wastewater with dangerous chemicals released during textile production. Textile maintenance often consumes even more energy and water than the production phase, and presents unique challenges in off-grid locations, disaster zones, during medical emergencies, or in other situations when frequent washing, drying, and re-use of fabrics are needed. Recycling of colored or blended textiles often presents a challenge for the waste-sorting near-infrared scanners, and most textiles end up in landfills or burned. Polyethylene (PE) has emerged recently as a promising polymer for wearable textiles owing to its high infrared transparency and tunable visible opacity, which allows the human body to cool via thermal radiation, potentially saving energy on building refrigeration. Here, we show that single-material PE fabrics may offer a high-performance sustainable alternative to conventional textiles, extending beyond radiative cooling. PE fabrics exhibit ultralight weight, low material cost, as well as recyclability. Industrial Materials Sustainability (Higg) Index calculations predict low environmental footprint of PE fabrics in the *production phase*. Via standard industry tests, we demonstrate efficient water wicking and fast drying performance of PE fabrics, which, combined with their excellent stain resistance, offer promise to reduce energy and environmental footprint of the textiles in their *use phase*. Unlike previously explored nano-porous PE materials, the high-performance PE fabrics in this study are made from fibers melt-spun and woven on the standard equipment used by the textile industry worldwide and do not require any chemical coatings. We also demonstrate that the PE fibers can be dry-colored during fabrication, resulting in dramatic water savings without masking the PE molecular fingerprints scanned during the automated recycling process.

The textile industry is a global commercial enterprise with market size valued at $961.5 billion in 2019,[1] producing an estimated 80 to 100 billion articles of clothing, or about 62 million tons each year[2]. It is also one of the most polluting and wasteful industries on earth, reputedly second only to oil and gas[3], consuming massive amounts of water for cotton production, and generating an estimated 11 million tons of textile waste annually the US alone[4,5]. Textile production is responsible for an estimated 1.2 billion metric tons of CO_2 equivalent (CO2e) per year, or 5-10% of global Greenhouse Gas (GHG) emissions[6]. The textile industry recognizes that it has a problem. It has adopted the UN Sustainable Development Goals (SDGs),[7] formed initiatives like the G7 Fashion Pact, but the impact on reducing the environmental footprint to date has been small.

The textile industry has long made use of natural fibers such as wool, cotton, silk, and linen, until the last century has witnessed rapid adoption of synthetic materials, including polyester, acrylic, and nylon. There is one common plastic, however, which – until recently – has been largely overlooked as a high-performance material for wearable textile production. This plastic is polyethylene, a low-cost and lightweight synthetic polymer. Polyethylene is one of the most-produced materials in the world, reaching annual production levels above 100 million metric tons, is cheap (see Supplementary Table S1), corrosion-resistant, easy to make, easy to recycle,[8–10] and can be converted into a new fuel source at the end of its lifespan[11]. Typically used in insulation, packaging and toy production[8], polyethylene also finds use in carpets and tarps. Non-woven polyethylene materials such as Tyvek® are used for lab wear and protective apparel for health workers and first responders, but they do not provide either functionalities or the level of comfort expected from everyday clothes or bedding textiles. Ultrahigh molecular weight (UHMWPE) fibers (such as Dyneema® and Spectra®), fabricated by the proprietary gel-spin processes, are very strong yet prohibitively expensive for everyday textile applications, finding use in e.g., bullet-proof vests, ropes and fishing nets.

Several years ago, we predicted theoretically that polyethylene can be a promising material for wearable textile production owing to its high transparency for long-wavelength infrared radiation emitted by the human body[12]. Infrared transparency of polyethylene garments may allow the body heat to escape radiatively, providing a passive cooling mechanism not available when using conventional textiles, which all exhibit high infrared absorptance. Visible opacity of polyethylene fabrics can be simultaneously achieved by engineering either the fiber or the pore sizes to scatter the short-wavelength visible light efficiently[12,13]. Follow-up experiments on nano-porous polyethylene films and fiber-based knitted textiles confirmed their passive cooling performance[13–16]. This property – unique for a polymer material suitable for wearable applications – provides a simple, low-cost solution to reduce energy consumption in HVAC systems[8,12], further elevating the sustainability profile of the polyethylene-based textiles.

Here, we show that polyethylene fabrics manufactured via standard textile industry processes and equipment offer competitive functional performance on many other measures beyond the passive radiative cooling functionality. In particular, we demonstrate that properly engineered woven polyethylene fabrics composed of multi-filament yarns can combine excellent stain resistance with efficient moisture wicking and fast-drying performance. As a result, woven PE fabrics are shown to exhibit passive evaporative cooling in addition to previously demonstrated passive radiative cooling, potentially translating into high level of personal comfort and further HVAC energy savings. In turn, stain-resistance and fast-drying functionalities of the PE fabrics offer significant energy savings in both domestic and industrial fabrics use via reduced temperature and time of

washing and tumble-drying cycles. Importantly, we show that the above functions can be achieved without treating PE fabrics with chemicals and without blending PE fibers with other fibers or sandwiching PE textiles with other fabric layers, which would have compromised the fabric recyclability. We also show that these properties can be maintained during the use phase via regular exposure to sunlight and friction occurring during the washing, drying and wear process. Finally, we demonstrate that polyethylene yarns can be colored via spin-dyeing (also referred to as either dope- or solution-dyeing) technique in an environmentally-friendly fashion, which eliminates the large amounts of potentially toxic wastewater created during conventional yarn dyeing processes. We also show that spin-dyeing of polyethylene fibers can be achieved with either conventional dyes or unconventional inorganic nanoparticle colorants, and allows for the automated infrared-scan sorting during recycling at the end of the material lifecycle.

Results

Upholding circular economy principles in textile industry requires the use of new raw materials that have a less environmental impact, upcycling existing plastic waste, as well as enhancing fabrics longevity and multi-functionality to promote re-use over recycling[17–19]. By using the data in the online Higg Materials Sustainability Index (MSI) database[20] (see Methods), we predict that the fabrication process of woven fabrics made of melt-spun PE yarn will exhibit the lowest environmental footprint among all common woven textiles, including cotton, linen (flax), wool, silk, nylon, and polyester (polyethylene terephthalate, PET). The data shown in Fig. 1a reveal that PE fabrics are expected to outperform conventional textiles by all indicators, including climate change, ozone depletion, human and ecosystem toxicity, particulate matter release, terrestrial acidification, freshwater and marine eutrophication, as well as fossil and water resource depletion.

Furthermore, it was recently demonstrated that polyethylene can be biologically sourced via fermentation of cellulosic sugars from waste biomass to ethanol, followed by its dehydration to ethylene and subsequent polymerization. This technology has been successfully commercialized by a number of companies including Braskem[21]. According to the measurement conducted by Carbon Trust and the Brazilian Technical Standards Association, polyethylene from renewable sources has a negative emission footprint (-2.11 kg of CO_2 equivalent per kilogram of product), i.e., it helps to sequester CO_2 from atmosphere. The use of bio-sourced PE can help to further reduce the environmental footprint of the PE fabrics production (Fig. 1a).

Supplementary Fig. S1 and Supplementary Table S2 summarize the contributions of different indicators to the overall environmental footprint of different textile types. Furthermore, the possibility of recycling the PE material (either mechanically or chemically) allows for additional reduction in the environmental footprint of polyethylene textiles[22]. Recyclability environmental gain indices of different materials compared in Fig. 1a[22] show that PE and polyester have the highest potential for recycling at the end of the material lifecycle.

The MSI Higg index only accounts for the environmental footprint of the material incurred during the production and end-of-lifecycle phases. However, studies show that textiles and garments may leave even larger environmental footprints in the course of their usage phase, by consuming energy, water, and chemicals during washing and tumble-drying processes[23–25]. In the following, we demonstrate that not only the new woven PE fabric has potential to significantly reduce environmental footprint in production, use, and end-of-lifecycle phases, but also it simultaneously offers high personal comfort.

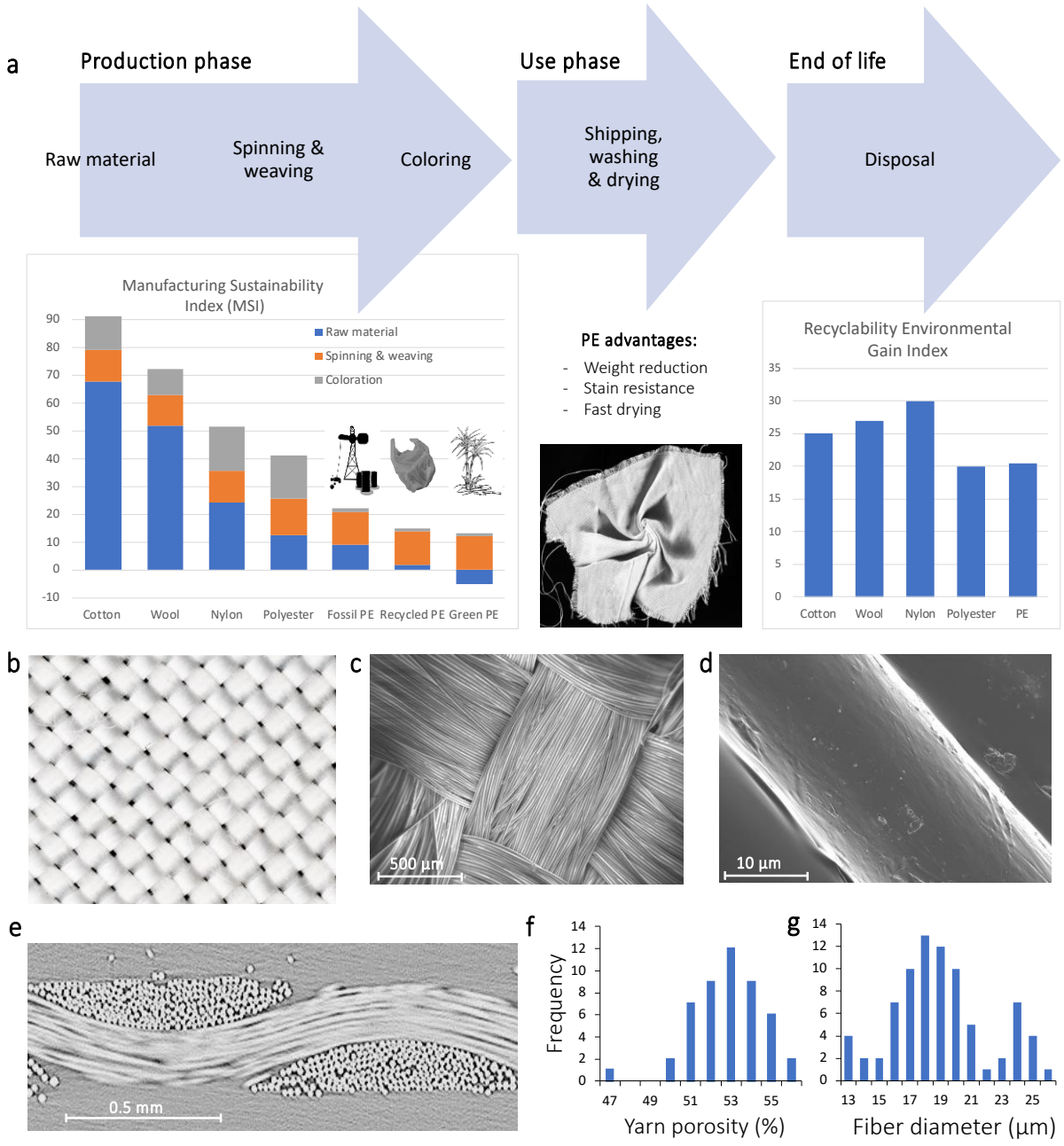

Figure 1. Polyethylene cast into the fiber form and woven into a fabric yields low-environmental footprint material for wearable textiles. (a) A schematic of the lifecycle of different fabrics, including comparative estimates of the environmental burden of each step. Production (cradle-to-gate) phase: non-dimensional MSI Higg indices, representing environmental footprints of 1 kg of PE woven fabric and of the same amounts of conventional woven textiles[20,21]. Use phase: the properties of the PE textiles demonstrated in this work offer reduction of the environmental footprint. End-of-life phase: Recyclability environmental gain indices of different materials[22]. Inset: Woven polyethylene textile fabricated on a standard industrial loom from linear low-density polyethylene (LLDPE) fibers produced by a standard melt-spin industrial process. (b) A high-resolution optical image, (c,d) scanning electron microscopy (SEM) images, and (e) a micro computed tomography (micro-CT) image reveal the details of the woven PE fabric composition and the fiber/yarn shape and size. (f,g) Frequency distributions of the yarn porosity (f) and the fiber diameters (g) evaluated on 48 yarn cross-section images and 100 individual fiber images, respectively, via SEM and micro-CT analysis. The average values are (53.0 ± 4.8) % and $(18.5 \pm 6.2)\ \mu m$, respectively.

Polyethylene can be cast in the form of continuous mono-filament fibers and multi-filament yarns via a simple process of melt extrusion (see Methods and Supplementary Figs. S2, S3). Polyethylene fabric shown in Figs. 1b-e has been woven on an industrial loom from a multi-filament yarn composed of 247 fibers of about 18.5 micron in diameter each (see Methods and Supplementary Figure S3). The yarn has been produced from a linear low-density polyethylene (LLDPE) material by a conventional melt-spin industrial process. Unlike previously demonstrated nano-porous polyethylene films and fabrics[13,15], the woven textile is neither mechanically reinforced by blending it with other fibers nor chemically treated to add a hydrophilic coating to the fiber surfaces.

The main micro-structure features of the woven PE fabric were evaluated by scanning electron microscopy (SEM) measurements (Figs. 1c,d) and via micro computed tomography (micro-CT) imaging techniques (Fig. 1e, Supplementary Video S1 and Supplementary Fig. S4). The average diameter of the PE fibers in the yarn is $(18.5 \pm 6.2)\ \mu m$ and they are arranged in a closely packed yarn with an average porosity of $(53.0 \pm 4.8)\%$ (see Fig. 1f,g and Supplementary Note 4). The fiber thickness and the dense woven pattern (plain - or tabby - weave) of the PE textile shown in Fig. 1 were chosen to optimize the efficient moisture transport and fast-drying performance of the material, and thus to promote higher comfort feeling and efficient passive cooling via evaporative process.

A common reservation to the use of polyethylene for wearable textiles stems from the inherent PE hydrophobicity, which is expected to prevent perspiration wicking. In Fig. 2, we demonstrate that this problem can be overcome by the proper textile engineering on the nano-, micro- and macro-scales (see Supplementary Video S2). We evaluated the water wicking capability of the woven PE fabric according to the AATCC 1977 standard, by partially submerging fabric samples into a water bath and measuring the height of the wet area forming in each sample 10 minutes after its exposure to water (see Fig. 2a and Methods).

Comparison to the corresponding wicking performance of several types of conventional fabrics revealed that the water wicking properties of the woven PE fabrics exceed those of natural (cotton and linen) and synthetic (polyester) commercial woven textiles with the same plain-weave pattern (Fig. 2b and Supplementary Fig. S6). This result seems counter-intuitive because polyethylene is known to be inherently hydrophobic, and PE films (including conventional low-density PE films and non-woven Tyvek PE material used in the experiment) are often used as waterproof covers and tarps (see Supplementary Fig. S7). As expected, the Tyvek sample did not exhibit any vertical water wicking in the AATCC 1977 test (Fig. 2b). The observed moisture wicking performance of the woven PE fabric is a result of a combination of the surface properties of individual fibers, the average fiber diameter, and the yarn composition.

The parameters determining the wicking process in a multi-filament yarn include: the water-fiber contact angle θ, the fiber radius r, the yarn structure, and the yarn porosity ϕ (Fig. 2c-e and Methods). The contact angle θ between the fiber and a distilled water droplet was measured to quantify the surface hydrophilicity of individual fibers (see Methods). The theoretical contact angle of pristine PE is approximately 94°, which would not allow the fiber surface wetting or a capillary suction in the yarn (see Supplementary Note 6). However, our data show that the surface of the melt-spun PE fibers is weakly hydrophilic, resulting in a reduced average water-fiber contact angle of $\theta = (71.3 \pm 3.3)°$, sufficient to promote wicking in the woven fabric (Fig. 2c, Supplementary Figs. S8 and S9, Methods and Supplementary Note 6). To eliminate the possibility of PE contamination by another material that would reduce the fiber surface energy, we confirmed the

purity of the chemical composition of the PE fibers by the Fourier Transform Infrared Spectroscopy measurements aided by the Attenuated Total Reflectance technique (FTIR-ATR, see Methods and Supplementary Fig. S10) and by the X-ray photoelectron spectroscopy (XPS, see Methods and Supplementary Fig. S11**)**. Our calculations confirm (Supplementary Note 6) that the water-fiber contact angle is not related to the fiber shape but is uniquely determined by the balance of the surface free energy at the three-phases contact line. Thus, the observed θ and the hydrophilicity of the PE fabric are due to a fabrication-process-induced increase of the surface free energy, by approximately 25% with respect to pure PE, which remains stable for 3-4 testing cycles (see Supplementary Note 9 and Supplementary Fig. S12).

The observed fiber surface hydrophilicity is a result of the fiber surface oxidation during the PE thermoforming by the melt-spin fabrication process in air, and is in line with prior observations of the water contact angles on ultra-high molecular weight polyethylene (UHMWPE) fibers.[26] Polymer thermoforming is known to not only oxidize the surface of the material but also to form initiation sites for future oxidation in the presence of oxygen even at ambient temperatures[27,28]. The XPS measurements revealed higher atomic concentration and molecular weight % of oxygen extracted from the XPS spectra of the PE yarn fabricated several months later than the yarn used to weave the PE fabrics (see Supplementary Fig. S11), confirming that the oxidation occurs at the fiber production stage.

Accordingly, the PE fiber surface oxidation can be further increased in magnitude and duration by additional fiber treatment, such as oxygen-plasma or UV-ozone, during or after the fabrication[29]. As an example, we measured the water-fiber contact angle on our PE fibers after treating them with oxygen plasma for 1, 3 and 10 minutes (see Methods and Supplementary Fig. S10a). As expected, we observed a reduction of θ by 14%, 23% and 27%, respectively. The FTIR-ATR spectra of the modified fibers accordingly show a slight increase in the infrared absorptance in the frequency range $1600\ cm^{-1} - 1700\ cm^{-1}$, corresponding to the spectral signature of the C=O stretching bond, and indicating the presence of the oxygen functional groups on the fiber surface[30] (see Supplementary Fig. S10b).

It should be emphasized that all the PE fibers characterized in this manuscript have been woven from as-drawn LLDPE multi-filament yarns without any specific surface treatment. We also observed experimentally that mechanical friction – a process that naturally occurs in the process of fabrics wearing, washing, and tumble-drying – restores the PE fabrics hydrophilicity, which we deliberately impeded by subjecting the fabric to eight wetting-drying cycles (see Supplementary Video S3). Finally, exposure of the fabric to UV light resulted in the partial restoration of the hydrophilicity impeded by wetting and drying processes (see Supplementary Fig. S13 and Supplementary Video S4), offering another mechanism of passive performance maintenance as a result of regular exposure to sunlight. Further optimization of the conditions of the fiber drawing and yarn weaving processes as well as follow-up studies on the synergistic effect of friction, sunlight illumination, and temperature variations on PE fabrics and garments may be needed to establish the optimum parameters for the material fabrication and care.

To understand, predict, and engineer the mechanisms of the moisture transport through PE yarns and textiles, we developed a model (see Methods and Supplementary Figs. S14-S18) of the liquid transport through capillaries in a multi-filament yarn[31,32]. In this model, the internal structure of the yarn is approximated as an infinite assembly of identical parallel fibers with circular cross sections, tightly packed into a periodic structure with identical distances between neighboring

filaments. The yarn is composed of non-ideally wetting fibers (i.e., with contact angles ranging from zero to 90 degrees) arranged in either a hexagonal (Fig. 2d) or a square (Fig. 2e) periodic lattice. To explain and optimize the PE yarn moisture transport functionality, which was experimentally observed in the vertical wicking test, we modeled water transport along the yarn in the direction parallel to the fibers axes. The along-the-yarn wicking process is considered dominant, as the ratio between the thickness of the fabric (perpendicular to fiber axis) and the length of the yarn (parallel to fiber axis) is on the order of 10^{-2}. The input parameters of the model are the fiber radius r, the yarn porosity ϕ and the water-fiber contact angle θ. The values of these parameters, which are used to make the model predictions, are obtained through experimental characterization (see Methods) and are equal to $2r = (18.5 \pm 6.2)\ \mu m$, $\phi = (53.0 \pm 4.8)\%$, and $\theta = (71.3 \pm 3.3)°$.

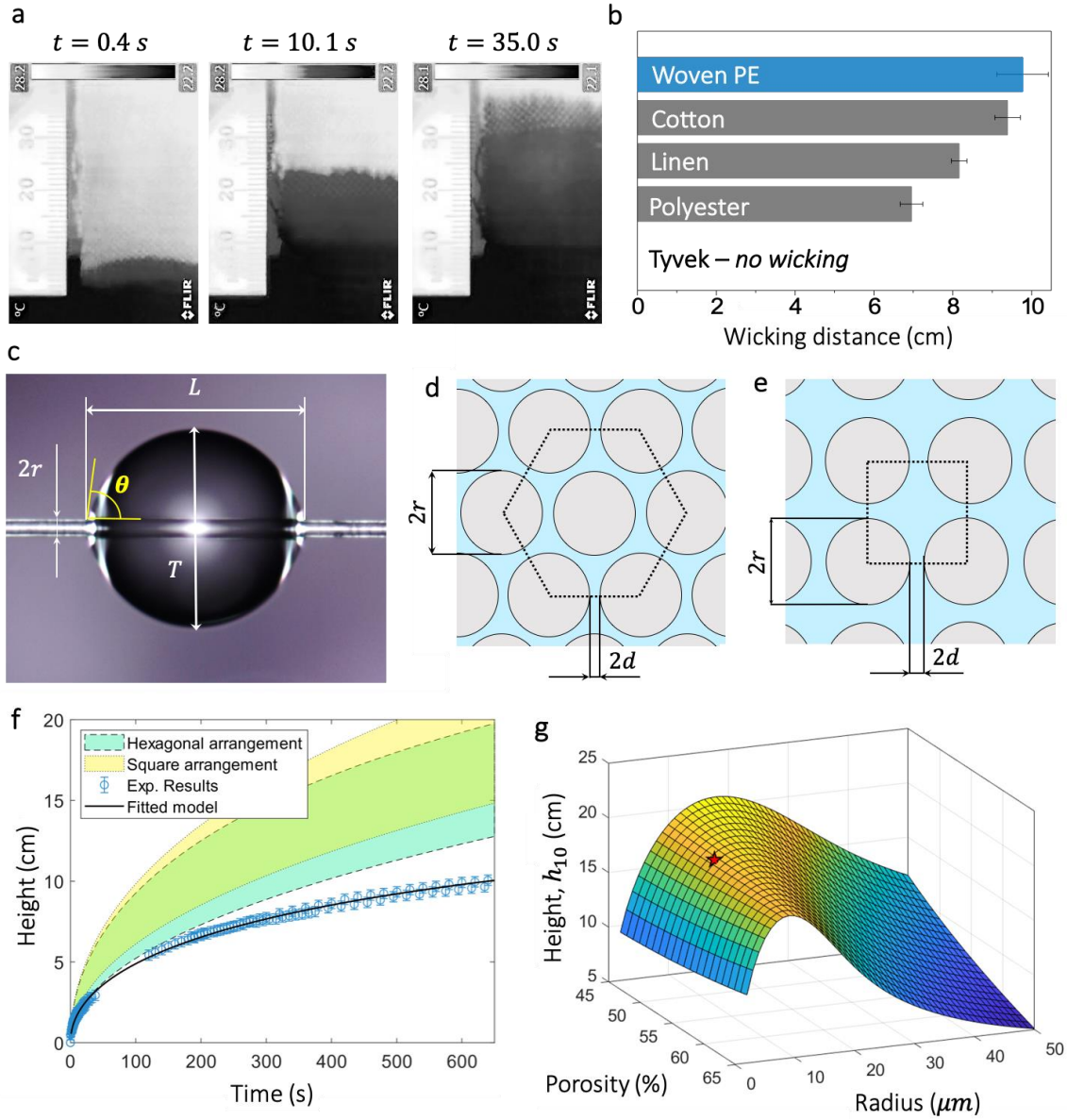

Figure 2. Wetting properties of the PE fabric, yarn, and fibers. (a) Infrared-camera images of a water-immersed woven PE fabric sample show the advancement of the transition line between the wet and dry regions at increasing times. (b) Vertical wicking distances in the woven PE fabric (blue bar) and in commercial woven textiles (gray bars) ten minutes after their contact with water. The corresponding data taken for the commercial non-woven PE material

Tyvek revealed no wicking action. (c) An optical image of a water droplet on a PE fiber and the contact angle parameters experimentally evaluated from the image. (d,e) Schematics of the elementary computational cells of a cross-section of an ideal yarn with a periodic hexagonal (d) or square (e) fiber arrangement. The grey circles represent the fibers composing the yarn. The water transport is modeled in the direction parallel to the fibers axes. (f) Comparison of the vertical wicking model predictions to the experimental results. The ideal model predictions (shaded areas) are calculated for yarns with the fiber diameters of $(18.5 \pm 6.2)\ \mu m$, contact angle of $(71.3 \pm 3.3)°$, and porosity of $(53.0 \pm 4.8)\%$. A single parameter comprising all the real yarn non-idealities was fitted on the experimental data set. (g) Fabric structure optimization to achieve efficient wicking: the height of the wet area in the ideal square-lattice PE yarn 10 mins after exposure as a function of the fiber radius and the yarn porosity for a fixed contact angle of $71.3°$. The red star represents the predicted performance of a yarn with the same combination of fiber radius and porosity as those experimentally evaluated for the PE woven fabric.

Figure 2f compares the model predictions of wicking action in the ideal hexagonal-lattice and square-lattice yarns with the experimental results of the vertical dynamic imbibition of the woven PE. The intervals of the model predictions for each ideal periodic-lattice yarn were computed within the experimental uncertainty of the fiber diameter, the contact angle and the yarn porosity. Since the real textile structure (see. Figs. 1b-e) is more complex than the simple linear model geometry, the ideal-yarn model overestimates the experimental performance of the woven PE textile. To account for the non-parallelism of the fibers in the yarn, the deviation from the ideal periodic pattern, yarn bending, a finite number of fibers in the yarn, and water evaporation occurring during the test, the model was modified by including a reduction coefficient (see Methods), fitted on the experimental data. The fitted model prediction for the square-symmetry ideal yarn with 60% performance reduction exhibited the best agreement with the experimental data in Fig. 2f as well as with the measured value of the maximum wicking height of $(13.8 \pm 0.8)\ cm$ measured in the woven PE fabric (see Methods).

The model was then used to predict the optimum fiber size and yarn configuration to achieve efficient moisture wicking action. Figure 2g illustrates that the optimum fiber radius and porosity in a square-lattice yarn composed of fibers with the contact angle of $71.3°$ are predicted to be approximately 15 μm and 45%, respectively. The optimum hexagonal-lattice yarn was predicted to have fibers of 20 μm in diameter and the porosity of 45% to achieve efficient wicking performance (see Supplementary Fig. S18). Although the wicking performance can be further improved by reducing the yarn porosity below 45%, the porosity range chosen in Fig. 2g and Supplementary Fig. S18 represents typical values for wearable woven textiles and provides a compromise between efficient capillary moisture transport and the fabric mechanical flexibility. The parameters of the PE multi-filament yarn used in this work (marked with a star on Fig. 2g) are not far from the optimum model predictions.

While the woven PE fabric is wicking moisture efficiently, water does not penetrate inside the PE fibers (see Supplementary Video S5), allowing it to evaporate efficiently from the fiber surface. In contrast, it is known that performance of natural fibers such as cotton and linen is hindered by the water absorbed and subsequently trapped within the fiber volume, which typically reduces the fabric drying rate.[33] To measure and compare the combined rate of moisture wicking and evaporation in different woven fabrics, we tested their drying performance by measuring the evaporation rate of a single droplet of water covered by a fabric sample according to the ISO 17617 standard (see Methods and Figs. 3a-c). This test allowed us to evaluate the performance of different fabrics under a testing condition similar to the perspiration wicking and evaporation from the fabric-covered skin surface. In this situation, moisture transport both across and along the fabric contributes to the droplet spread and evaporation. Note that due to the structure of the

woven fabric (see Fig. 1e, Supplementary Figs. S3 and S4, and Supplementary Video S1), efficient moisture wicking in the direction along the yarn not only helps to spread the droplet laterally but also promotes vertical moisture transport across the fabric to its top surface.

Comparison of the data for the vertical test wicking distance (Fig. 2b) and the horizontal test drying rate (Fig. 3d) show that while woven PE fabrics outperform other tested textiles on both measures, the materials that exhibit good wicking performance may underperform significantly in the combined wicking-drying test. This situation is observed for textiles made of natural fibers such as cotton and linen due to their moisture-trapping properties.[33] In contrast, the very slow drying rate measured for the non-woven Tyvek PE film is predominantly influenced by the material hydrophobicity, which inhibits water wicking, traps water under the textile, and ultimately slows down the evaporation process. This combination of the observed fast wicking and the subsequent fast evaporation exhibited by the woven PE fabric is generally advantageous for applications in wearables and bedding, promoting both personal comfort feeling and the evaporative cooling functionality. It also offers an opportunity to reduce both the temperature and the duration of the tumble-drying cycle, resulting in energy savings and lowered environmental impact.

Fabrics that promote efficient moisture transport and evaporation offer a passive way of cooling the human body (or any surface they cover) via the process of evaporative cooling. To measure and compare the evaporative cooling performance of different fabrics, we recorded the temperature distribution underneath different types of drying fabrics over time. Essentially, the evaporation test of the ISO 17617 standard was repeated by replacing the Petri dish with a hydrophobic and thermally insulating surface mimicking the human skin, which had four equidistantly embedded thermistors (see Fig. 3e). The water droplet was introduced on top of the central thermistor and then covered with a textile sample. The radial temperature distribution on the simulated skin was evaluated by recording the input from all the four thermistors, exploiting the axial symmetry of the water front propagation. Efficient moisture transport along the woven PE textile followed by the efficient evaporation process yielded fast droplet spreading, maximizing the evaporation surface and providing a uniform temperature distribution on the skin under the wet area. As a result, the drying rate of the sessile droplet on the simulated skin covered by the woven PE fabric has been measured to be 3.2 times higher than on a bare skin surface. As shown in Fig. 3f, all the four thermistors registered sharp initial temperature drop, followed by even sharper reverse transition as the temperature returned to its initial value upon complete evaporation of water. The steep slope of the initial temperature drop is the result of the fast water front propagation and simultaneous fast evaporation, while the steep slope of the temperature recovery process is due to the PE hydrophobicity, which prevents water capture inside the PE fiber volume and thus thermal inertia.

In stark contrast, cotton (Fig. 3g and Supplementary Fig. S20) and linen (Supplementary Fig. S19) exhibited slower initial temperature drops and much longer temperature recovery times, with the areas further away from the fabrics center cooling down less than the center. The observed performance is once again governed by the water absorption inside the volume of natural fibers, which hinders initial propagation of the water front, reduces the evaporation surface, and slows down the evaporation process. This property increases the drying time of natural textiles, reduces comfort, and leads to longer times and higher temperatures of tumble-dry processes, thus increasing energy consumption[23]. The polyester fabric exhibited evaporative cooling performance intermediate between those of the woven PE and natural textiles, while the effectiveness of evaporative cooling of Tyvek-clad and bare skin surfaces was severely hindered by the lack of

moisture wicking and spreading via capillary transport, leading to a reduced evaporation rate and uneven temperature distribution on the surface of the skin (Supplementary Fig. S19).

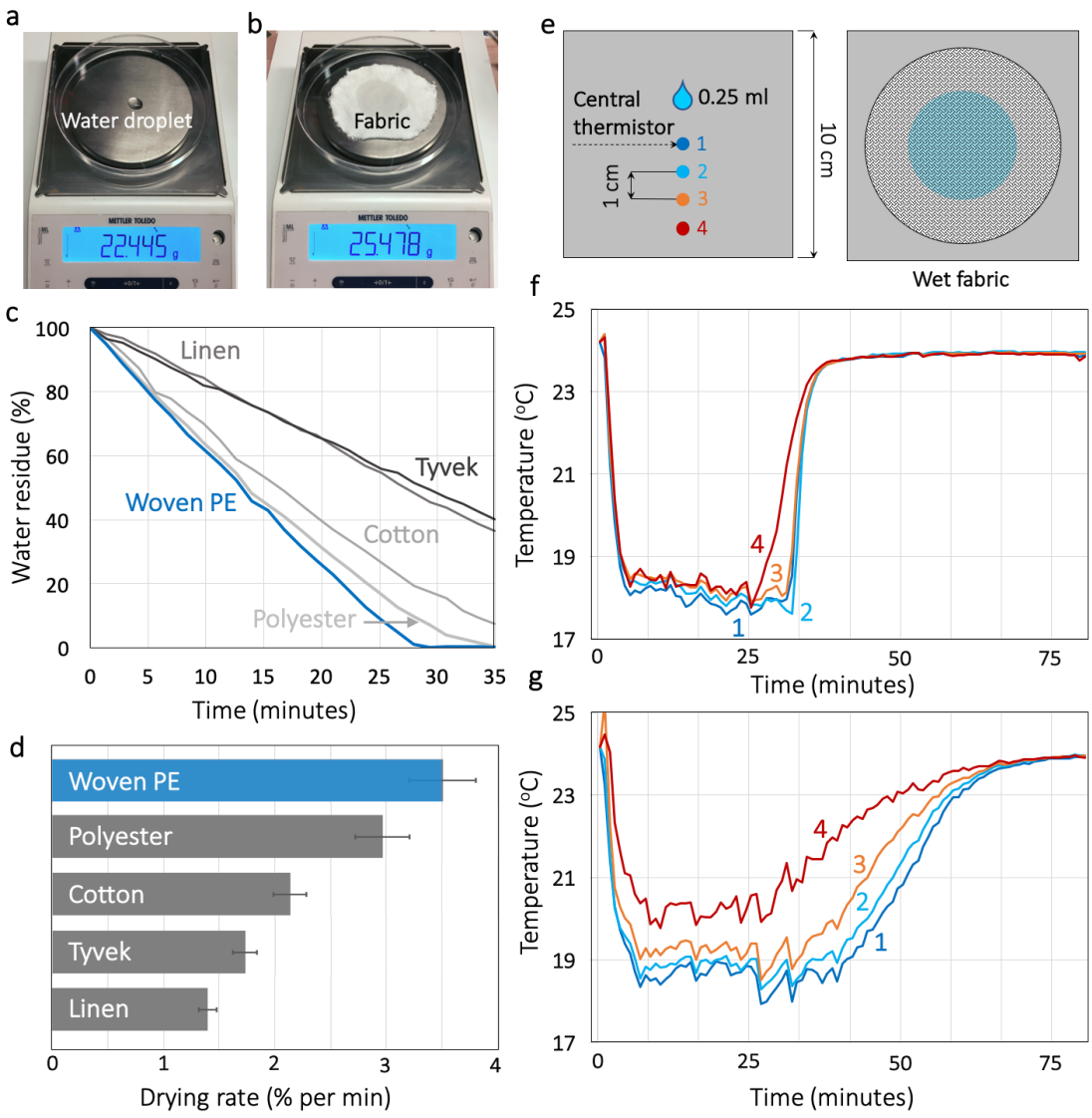

Figure 3. Comparative drying and evaporative cooling performance of textiles. (a,b) Photographs of the experimental setup used to measure the drying rate of textiles according to the ISO 17617 standard with modifications. (c,d) Drying rate of the woven PE fabric and conventional textiles. The drying rate of the commercial non-woven PE material Tyvek is also shown for comparison. (e) Schematics of the experimental setup used to measure the lateral moisture spreading and evaporative cooling performance of textiles (top view). (f,g) Temperature measurements underneath woven PE (f) and cotton (g) fabrics covering a drop of water deposited on top of thermistor 1.

The hydrophobicity of pristine polyethylene stems from the lack of ionic bonds or polar molecular groups on the PE macro-molecule for water molecules to attach to (see Fig. 4a). The same properties of the PE macro-molecule prevent soiling and degradation of polyethylene materials due to exposure to organic and inorganic contaminants, including acids and alkalis[34]. Although slight oxidation of the melt-spun fiber surface enables achieving weak hydrophilicity of the PE fibers and textiles, our tests show that the woven PE fabrics retain stain resistance properties typical for pristine PE materials. Figure 4 compares stain resistance of the woven PE fabric to those of the conventional textiles. As illustrated in Figs. 4a-c, the molecular structures of polyethylene terephthalate (polyester) and cellulose (cotton and linen) are significantly more complex than

those of polyethylene and feature multiple sites available for strong attachment of dyes, dirt, and microorganisms.

Figure 4d shows dry textile samples (top row), the same samples stained with a food colorant (middle row), and the stained samples washed by rinsing them with cold tap water for 30 seconds (bottom row). Simple cold-water rinsing of the PE textile resulted in the complete stain removal. In contrast, cotton, linen, and polyester fabrics remain stained after undergoing the same staining/washing procedure, with natural fabrics exhibiting the most persistent stains. This stain-resistance property of polyethylene is expected to inhibit accumulation of dirt and microorganisms in PE textiles, and can help to reduce the consumption of energy, time, water, and detergent during the fabrics use phase.

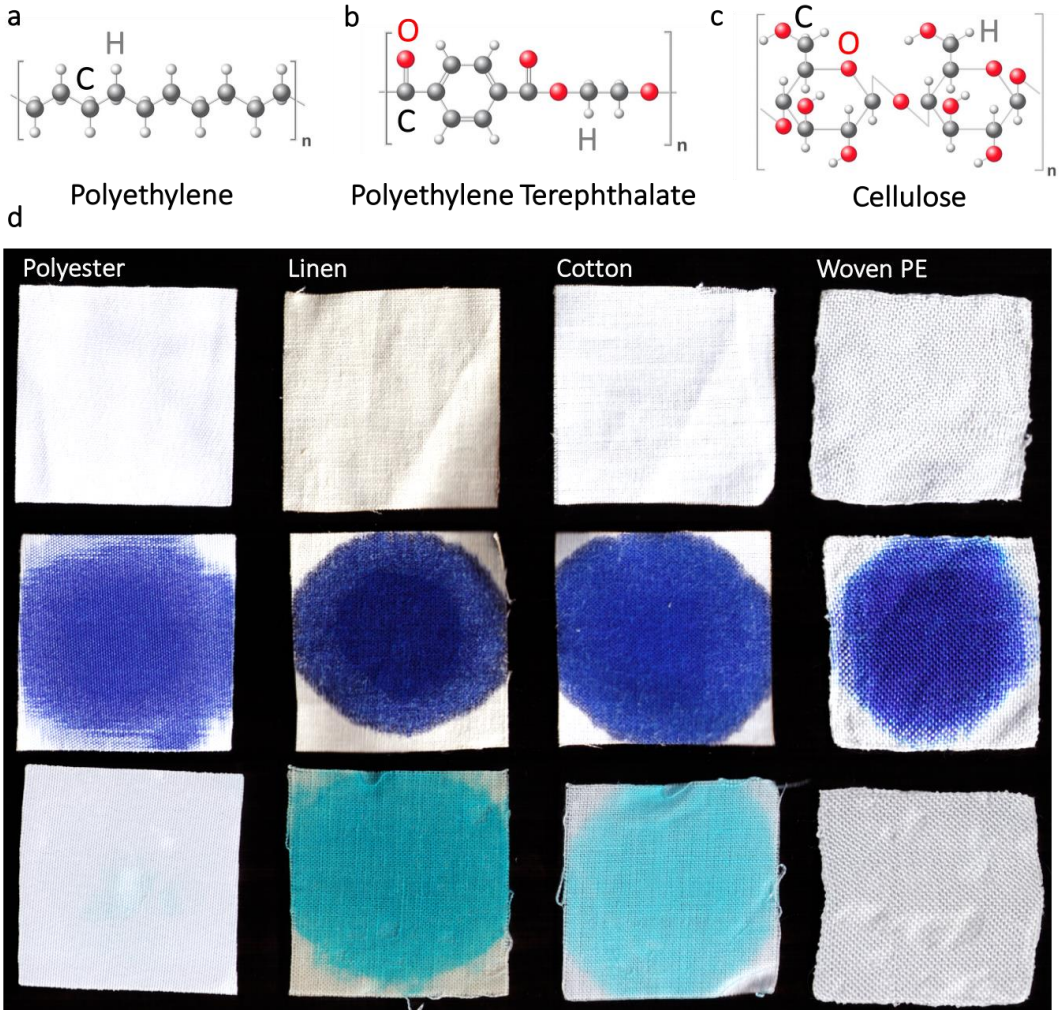

Figure 4. Simple structure of polyethylene molecule inhibits PE fabrics staining and simplifies washing procedure. (a) Polyethylene molecule is comprised of a carbon backbone surrounded by satellite hydrogen atoms, without ionic bonds or polar groups. (b,c) Polymer molecules of polyethylene terephthalate (polyester) and cellulose (cotton and linen) exhibit multiple sites available for the attachment of dyes and contaminants. (d) Photographs of woven fabric samples stained by a commercial food colorant and subsequently rinsed under the running cold tap water without the use of soap or any chemicals. Complete removal of the stain from the PE textile was observed after approximately 30 seconds of rinsing time. The photos of other fabric samples before (top) and after (bottom) rinsing reveal the stains persisting after the rinsing procedure.

However, this stain-resistance property also makes it impossible to color polyethylene textiles by conventional dye-dipping techniques[34], and historically hindered its applications in the textile and fashion industry. While there are many markets available for uncolored (white) PE textiles, including underwear, bedding, tableware, bandage materials, wastewater treatment filters, etc., other applications require colored fibers and fabrics. To address this issue, we have developed a process for embedding colorants into the PE fibers during their fabrication by melt-spinning, which can produce a variety of colors (Fig. 5a). This spin-dyeing process does not require water use, and generates colored fibers with colorants firmly trapped between polymer chains, offering promise for good color fastness performance. It also allows the use of non-conventional materials as colorants, including inorganic micro- and nano-particles along with conventional organic dyes[35,36]. The red and blue PE fibers in Fig. 5a have been colored by embedding disperse dyes into the fiber, while brown color has been achieved by doping the fiber with 100 nm-diameter Si nanoparticles (see Methods).

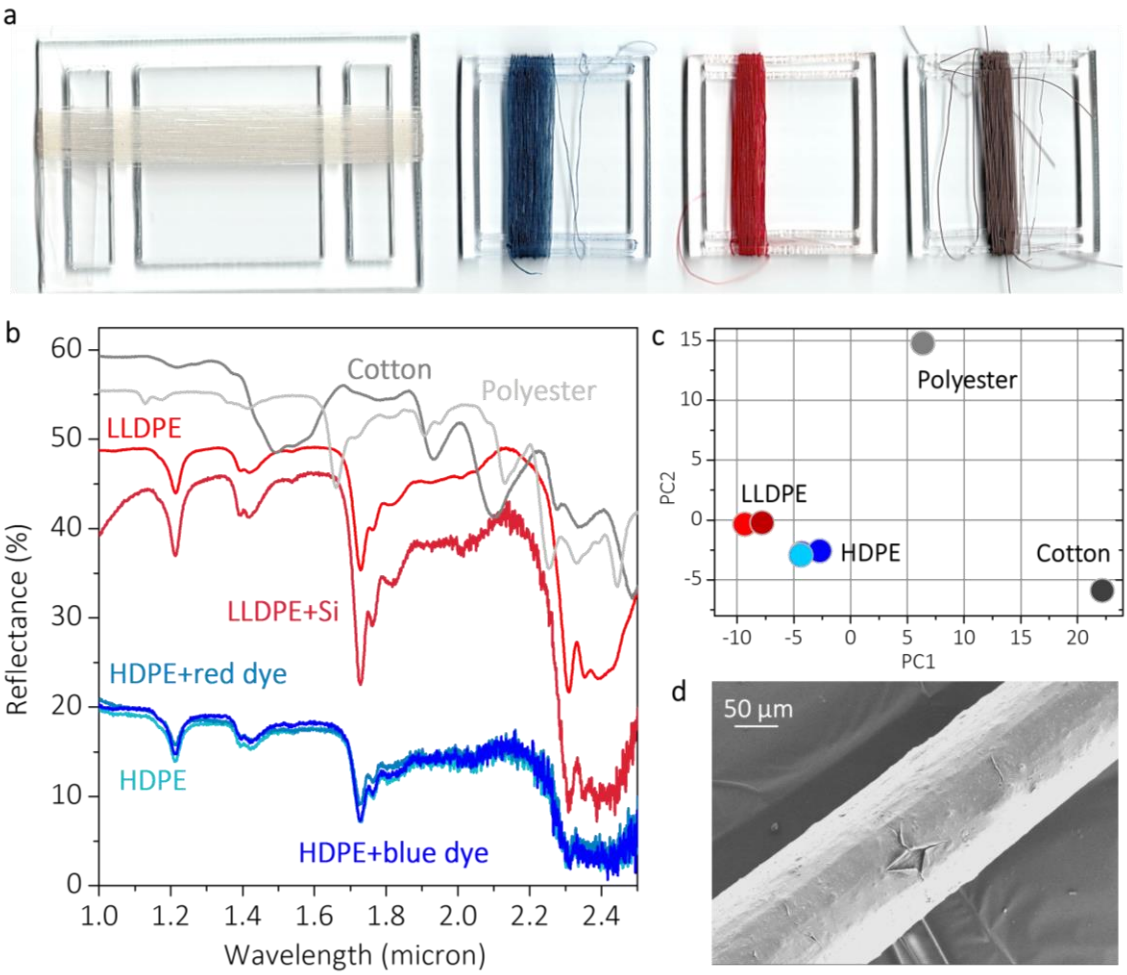

Figure 5. (a) Examples of the PE fibers with and without embedded colorants, including red and blue disperse dyes, and Si nanoparticles. (b) Optical reflectance spectra of the colored and non-colored PE fibers in the near-infrared range compared to those of cotton and polyester fabrics. (c) The results of the principal component analysis of the spectra in panel b, which reveal the opportunity to automatically sort both colored and non-colored PE textiles by their spectral fingerprints during the recycling process. (d) An SEM image of the blue PE fiber with the embedded dye powder, illustrating its stable capture by the polymer matrix, which reduces the risk of performance degradation and environmental hazard associated with the dye release into the environment.

The measured near-infrared spectra of colorless (white) and colored fibers with embedded organic and inorganic coloring agents shown in Fig. 5b (see Methods) reveal that the presence of the colorant does not obscure the characteristic near-infrared spectral features of polyethylene, which are distinctly different from those of cotton and polyester. These 'spectral fingerprints' are overtones and combinational bands of the molecular vibrational modes associated with stretching deformations, and are typically used to distinguish and sort different types of materials during the automated recycling process[30]. The principal component analysis of the near-infrared spectra of all the materials shown in Fig. 5b (see Methods and Supplementary Fig. S21) reveals that the fibers made of the same base material type (i.e., LLDPE, HDPE, cotton, and polyester) can be easily distinguished from each other by their spectral fingerprints regardless of the presence of the embedded colorants (Fig. 5c). Polyester plastic waste is already being recycled into the industrial fiber form, and we expect that similar process can be easily established for the waste PE recycling. Finally, Fig. 5d shows an SEM image of a fiber exhibiting visual coloring due to the embedded blue disperse dye and demonstrates safe encapsulation of dye into the fiber matrix, holding promise for a good color fastness of the PE fibers and textiles.

Discussion

Polyethylene is one of the most-produced materials in the world[37], and is fully recyclable, either mechanically via a melt-extrusion process or chemically via solvent dissolution and pyrolysis (material breakdown at high temperatures in the absence of oxygen)[9,10]. However, most of PE waste ends up being incinerated, as it is not economically viable to recycle it in the form of low-cost plastic bags and films. New types of high-value products made from PE – such as fabrics and wearables – can make its recycling profitable and help to close the material lifecycle[17,19]. The LCA analysis predicts (Fig. 1 and Supplementary Fig. S1) that even the use of virgin fossil-derived PE material for textile production can help to reduce the environmental footprint of the textile industry, with recycled material offering further reduction of energy needs, CO_2 release, and environmental damage. These predictions are supported by the results of the recent study on the environmental impact of the grocery bags conducted by the Danish Environmental Protection agency[38], which also identified LDPE bags as the most environment-friendly option. Bio-derived PE material offers further environmental footprint reduction and is still fully recyclable at the end of its lifecycle.

This study further suggests that the use of polyethylene offers potential for significant reduction of environmental footprint of textiles not only in the production phase, but also during the use phase. In particular, the demonstrated stain-resistance of the woven PE fabric can help in reducing the use of water, energy and chemicals during its wash cycle, while the observed fast fabric drying performance is advantageous for reducing the energy consumption and the amount of waste heat generated during the tumble-dry cycle. In comparison, a breakdown of energy consumption during the four major phases in the life cycle of a cotton T-shirt (i.e., material/production, transportation, use, and disposal) shows that over 70% of energy is consumed in the use cycle (mostly for high-temperature washing and tumble-drying)[23].

The evaporative cooling functionality of PE fabrics revealed and quantified in this study not only allows to shorten (or even completely eliminate) the tumble-drying cycle but also provides an additional powerful mechanism to achieve thermal comfort both indoors and outdoors. This mechanism can be exploited in the engineering of high-performance athletic apparel for professional sports, farming and gardening, military use, and recreational outdoor activities to

reduce thermal stress and improve performance. Furthermore, the efficient evaporative cooling of woven PE fabrics demonstrated in this study, together with their previously discovered passive radiative cooling functionality, can help to reduce the HVAC energy consumption in hot climates or during the peak summer season[8,12,13,15]. Passive evaporative cooling and anti-fouling properties of PE textiles can also be leveraged for applications beyond the wearables and consumer textiles, e.g., to improve performance and increase durability of passive water purification platforms[39,40] or to cool produce in remote off-the-grid locations[41].

Polyethylene internal properties can be dramatically varied by engineering the polymer chain length and branching as well as by the control of the material crystallinity[8]. Through a combination of mechanical, X-ray, and thermal characterization of the PE fibers and fabrics (see Supplementary Figs. 22-24 and Supplementary Tables S5,S6), we demonstrated control over the fiber tensile strength, melting temperature, and abrasion resistance via internal polymer properties and external fabric structure properties. In turn, the tested handle-feel properties of the woven PE textiles revealed that they exhibit high softness and flexibility relative to other tested materials, with high recovery after compression (Supplementary Table S7). Importantly, all the PE fibers exhibiting a wide range of tensile strength properties have been fabricated by standard melt-extrusion. This sets them apart from commercially available high-strength high-cost UHMWPE fibers (such as Dyneema and Spectra), which are fabricated by the proprietary gel-spin process. All the PE fibers and yarns used in this work can be woven and knitted by using standard industrial equipment, and fabrics with different woven/knitted patterns can be engineered and tailored for a specific application (see Supplementary Fig. S25).

Polyethylene is biologically inert and can be softened without plasticizers. Owing to its chemical inertness, polyethylene is considered safe for use in cosmetic formulations, and is one of the most common materials used in medical implants because it does not degrade in the body[42,43]. As we demonstrate here, PE yarns can be spin-dyed with a variety of organic and inorganic colorants, which can be carefully chosen to reduce the potential health risks[44]. Although polyethylene has long been shunned by the textile producers due to its resistance to traditional dyeing techniques, the performance apparel industry is increasingly embracing the spin-dyeing technology (long used in carpet production) as the means to reduce the textile environmental footprint and to significantly improve the fabrics color fastness to washing, drying, and light exposure[45–47]. The spin-dyed PE yarn color fastness is expected to further reduce environmental and health risks by limiting the colorant release to the environment, and to expand the garment life span[34].

We would finally like to emphasize that all the passive cooling and stain-resistance functionalities of PE fabrics discussed in this work have been achieved by meso-scale engineering of the structure of polymer fibers, yarns, and knitting/woven patterns, and do not require blending PE with other materials or covering its surface with chemical coatings. The nanoparticle colorants added for aesthetic purposes can be removed from the colored PE textiles during the recycling process, e.g. via centrifuging or filtering. In contrast, commercially-available fabrics with evaporative cooling performance are typically composed of two or three layers of different polymer materials, often with additional coatings, which complicates and often prevents their recycling. Finally, most fashion accessories such as buttons, hooks, zippers, and labels can also be made from polyethylene, enabling a single-material platform ideal for efficient automated recycling at the end of the garment life cycle. While material degradation of discarded PE textiles can be a subject of a separate study, a clear recycling pathway for PE fabrics and garments is expected to reduce the probability of them ending up in landfills and contributing to the microplastic pollution. It can also

offer an opportunity to recycle the previously accumulated large amounts of LDPE waste, whose recycling is currently not economically viable due to the lack of added-value LLDPE products. The single-material polyethylene-based multi-functional and circular fabric platform could offer unique advantages for a wide range of applications and consumer markets in textile industry and beyond.

Methods

Fabrication of PE fibers, yarns, and woven fabrics

The polyethylene fibers and yarns used in this study have been fabricated by the standard fiber melt spinning process from the linear low-density polyethylene (LLDPE) and high-density polyethylene (HDPE) granules and pellets (Alfa Aesar). The monofilament fibers of varying diameters have been fabricated at the US Army CCDC Soldier Center (Natick, MA) by using a conical miniature twin-screw extruder (MicroCompounder, DACA Instruments). The multi-filament LLDPE yarns have been fabricated by the MiniFibers Inc. (Johnson City, TN) on an industrial-scale melt-spin extruder. The yarns are composed of 247 individual filaments with 2 dpf (denier per filament). The yarns have been woven into a plain-weave textile on an industrial-scale loom at the Shingora Textile Ltd. (Ludhiana, Punjab, India). The monofilament fibers have been dry-colored via the spin-dyeing process, by mixing the colorants with the PE material prior to the fiber melt extrusion. The colorants used in this study included commercial disperse dyes (Millipore Sigma) and silicon nano-powders (US Research Nanomaterials Inc.), see Supplementary Note 2.

Structural characterization of fibers, yarns, and fabrics

The microscopic structure of the PE fibers and fabrics has been characterized with a high-resolution scanning electron microscope (HR-SEM, Zeiss, model Merlin). To obtain the cross-sectional view of the woven fabric and estimate the average fiber radius, inter-fiber capillary size, and yarn porosity, the fabric samples were scanned in a high-resolution micro-CT scanner to a pixel size of 2 µm (Zeiss Xradia 620 Versa, 0.4x objective). For further detail, see Supplementary Notes 3 and 4.

Characterization of the wicking performances of the fabrics

The wicking rates of various fabrics presented in Fig. 2b were estimated via a vertical wicking test according to the AATCC 1977 standard. The bottom ends of vertical fabric specimens were partially submerged in the bath filled with distilled water, and the wicking distance was measured after a 10-minutes period. Infrared camera images (FLIR ETS320) were used to identify the transition point between the dry and wet portions of the fabrics, and a caliper (Anytime Tools dial caliper 6") was used to measure the wicking distances. See Supplementary Note 5 for more details and for the procedure used to measure the maximum capillary height.

Water-fiber contact angle characterization

The water-fiber contact angle θ was computed by measuring the ratio between the maximum length and the thickness of droplets deposited on a PE fiber and the fiber radius (see Fig. 2c)[48,49]. The fibers were extracted from yarns randomly picked from woven PE fabric samples, and fixed with tape between two glass slides. Water was sprayed on the fiber to allow the deposition of

droplets on its surface. A confocal microscope coupled to a Raman spectrometer (Horiba, LabRAM HR Evolution) was used to photograph the droplets deposited on the fiber. A maximum of two droplets were photographed on each fiber before replacing the sample. The contact angle was calculated by averaging the data from 16 separate measurements. See Supplementary Notes 6 and 7 for more detail.

Spectral characterization of fibers and fabrics

The spectral characterization of fabrics in the wavelength range between 250 nm and 2500 nm was carried out by using a UV-Vis-NIR spectrophotometer Agilent, model Cary 5000, equipped with an integrating sphere in which samples were placed in the reflectance port (scan rate of 600 nm/min). The surface chemistry of fibers comprising the woven PE fabrics was probed via the Fourier Transform Infrared (FTIR) spectroscopy, using the Attenuated Total Reflectance (ATR) mode. For this, a Nicolet 6700 spectrometer equipped with a Nicolet Continuμm Microscope with an ATR objective equipped with a Germanium crystal was used. ATR-FTIR spectra were collected in the range 4000-650 cm^{-1} at resolution of 4 cm^{-1} and were averaged over 32 scans. We have performed additional analysis of the surface oxidation of the PE fibers by using the X-ray photoelectron spectroscopy (XPS). We have used the Physical Electronics Versaprobe II X-ray Photoelectron Spectrometer to perform elemental and chemical spectroscopic analysis of fiber surfaces. Monochromatic Al Kα radiation (hv = 1486.6 eV) was used as the excitation source to analyze the different binding energy peaks (pass energy 11 eV, analyzer resolution ≤0.5 eV). For further detail, see Supplementary Note 8.

Theoretical model of water transport along the yarn (parallel to the fibers axis)

The ideal yarn structure was simulated as an array of identical, parallel cylinders forming periodic hexagonal or square lattices (Figs. 2d,e). The model can predict the time-dependent height of the water front in a fabric sample during vertical imbibition, ignoring the effect of the water evaporation. The dynamic imbibition of a single-phase fluid (water) in a rigid porous material (yarn) under isothermal condition was modelled by combining the Darcy's law and the continuity equation[50]:

$$\nabla \cdot \left(-\frac{K}{\mu} (\nabla \langle p_w \rangle + \rho g) \right) = 0 \,, \tag{1}$$

where K is the permeability of the fabric, μ is the dynamic viscosity of the wetting fluid, ρ is the density of water, g is the gravitational acceleration, and $\langle p_w \rangle$ is the pore-averaged pressure of the fluid. A one-dimensional equation for the position h of the advancing water front was derived using the following boundary conditions:

$$\begin{aligned} p_w &= p_{atm} \ \text{ at } \ h = 0 \,, \\ p_w &= p_{atm} - p_c + \rho g h_t \ \text{ at } \ h = h_t \,, \end{aligned} \tag{2}$$

where $p_{atm}$is the atmospheric pressure, p_c is the capillary pressure, and h_t is the position of the water front at time t. Finally, the implicit equation describing the advancement of the water front is [50]:

$$p_c \ln \left| \frac{p_c}{p_c - \rho g h_t} \right| - \rho g h_t = \frac{\rho^2 g^2 K}{\phi \mu} t \,. \tag{3}$$

This equation shows that the wicking properties of a textile are determined by three parameters: the yarn porosity ϕ, the microscopic permeability K and the capillary pressure p_c. The yarn porosity was evaluated from the micro-CT characterization as $\phi = (53.0 \pm 4.8)\%$. The microscopic permeability K along the fiber axis is a function of ϕ and ϕ_{min}, where the latter is the minimum porosity of the yarn and is uniquely determined by the supposed fibers arrangement (namely, square or hexagonal). The model used to evaluate K is described in Supplementary Note 10. The capillary pressure $p_c = \rho g h_{max}$ is a function of the maximum capillary height along the fiber axis h_{max}, which was evaluated following the modelling approach proposed by Princen[31,51] (see Supplementary Notes 11 and 11.2). The limits of validity of the model are described in Supplementary Note 11.3. The effect of the input parameters on h_{max} and on h_t is described in Supplementary Note 11.4. Considering all the parameters involved in Eq. 3, the whole transport model is only a function of the geometrical parameters r, ϕ and of the contact angle θ.

The non-ideality of the real yarn was accounted for via a single coefficient A, included to reduce the capillary pressure: $p_c = \rho g (A \cdot h_{max})$. For both fiber arrangements, the reduction coefficient A was scanned through 30 equidistant points in the range $0.3 \leq A \leq 0.5$, and the other model parameters (namely, ϕ, r, and θ) were consequently fitted on 171 experimental data points obtained from five different vertical wicking tests. The fitting was performed by minimizing the root mean squared error (RMSE) between the modeling prediction and the experimental data set. The best fit for the hexagonal fiber arrangement was obtained with $\phi_H = 0.554$, $2r_H = 21.6\ \mu m$, $\theta_H = 73°$ and $A_H = 0.46$, while the coefficients fitting the data with a square yarn symmetry are $\phi_S = 0.554$, $2r_S = 20.1\ \mu m$, $\theta_S = 71°$ and $A_S = 0.36$. For both arrangements of fibers, the fitted values of porosity and contact angle are within 5% with respect to the average experimental value, while the fitted value of the fibers diameter are 13% and 17% larger, for the square and hexagonal arrangements, respectively. The result is consistent with the large uncertainty related to the experimentally-measured fiber radii. Given that the maximum height fitted for the hexagonal arrangement is 7% larger than the experimental value and outside its confidence interval, the periodic square-lattice model of the yarn was adopted for the woven PE fabric wicking performance optimization in Fig. 2g.

Characterization of the moisture drying properties of fabrics

The drying properties of the fabrics were measured via the ISO 17617 standard (method B) with modifications. The circular fabric test specimens (85 ± 2) mm in diameter were kept at the room temperature and relative humidity of (40 ± 5) %, measured with a hygrometer (RH820, Omega instruments), for one day. The ambient temperature was monitored with a thermistor (model 4033, Omega instruments) and maintained at (23.6 ± 0.3) °C. Each sample was laid in a Petri dish placed on a precision balance (Mettler Toledo, NewClassic ML), weighed and removed. Then, (0.25 ± 0.02) ml of distilled water was applied using a micropipette to the center of the base of a Petri dish and covered by the test fabric specimen. The whole setup was exposed to the environment (Fig. 3a,b), whose temperature and humidity are measured during the experiment. The weight loss caused by the water evaporation was measured for 2 minutes. With these data, the drying time and drying rate (% per minute) were calculated using the least squares fitting method (see Supplementary Table S3). For further detail, see Supplementary Note 12.

To evaluate the effect of the evaporation on the spatial temperature distribution, the evaporation tests were repeated by substituting the Petri dish with a polystyrene plate 10x10 cm wide and 2 cm thick. A thermistor (model 4033, Omega instruments) was placed at the center of the specimen

surface. Three other thermistors were positioned in radial direction from the central one with an equal spacing of 1 cm (Fig. 3e) and covered with a water-resistant tape, to prevent the direct contact between the distilled water and the sensing elements. The distilled water basin was kept on a heated magnetic stirrer to maintain the temperature difference between the reservoir, measured with a properly insulated thermistor, and the average temperature of the plate surface within 0.2°C. The micropipette was kept immersed in the reservoir to achieve thermal equilibrium with water. All the data from the thermistors were acquired with a digital data logger (OM-CP-OCTPRO, Omega instruments) using a sampling frequency of 1 sample/s.

Principal Component Analysis (PCA) of the fabrics near-infrared spectra

The experimentally-measured total (specular and diffuse) reflectance spectra in the range from 1 micron to 2.5 micron were evaluated by the principal component analysis. The PCA analysis was performed using package "stats" in R environment (v. 3.6.1)[52]. The reflectance spectral data were converted to z-scores prior to PCA analysis. Analysis showed that 65% of the variation between the near-IR spectra was accounted by the first principal component (PC1) and 25% by the second principal component (PC2), which were used to produce the PCA scatter plot in Fig. 5c. See Supplementary Note 13 for additional detail.

Thermal, mechanical, and crystallinity characterization of the PE fibers and fabrics

Abrasion testing of the textiles has been done on the Martindale M235 Abrasion Tester according to the ASTM D 4966 standard (see Supplementary Fig. S22). Tensile strengths of the PE fibers have been measured by using an Instron 68SC-05 and a KLA T150 UTM tester (see Supplementary Fig. S23 and Supplementary Table S5). The fabric touch tester (FTT) equipment (SDL Atlas) has been used to evaluate the handle feel properties of the woven PE fabrics (see Supplementary Table S7). Crystallinity of the PE fibers studied in this work has been measured via differential scanning calorimetry (DSC, model Discovery from TA Instruments) and via the wide-angle X-ray scattering (WAXS) technique (SAXSLAB system with a Rigaku 002 microfocus X-ray source and a DECTRIS PILATUS 300K detector). The data are summarized in Supplementary Notes 14 and 15.

Estimation of the experimental uncertainty

The estimation of the uncertainty of the measures presented in this work is reported in Supplementary Note 18.

Acknowledgements

This work has been supported by the CCDC Soldier Center (via the MIT Institute for Soldier Nanotechnologies), the Advanced Functional Fabrics of America (AFFOA) institute, MIT International Science and Technology Initiatives – MISTI (MIT - Italy MITOR Project 2018), the Deshpande Center, MIT-Tecnológico de Monterrey Nanotechnology Program, and the UNSW-USA Networks of Excellence. The authors thank John Garner (Minifibers Inc.), Anuj Jain (Shingora Ltd.), Mary Jane Schmuhl (AFFOA), and Betty Ann Welsh (CCDC-SC) for help with the PE fiber and textile fabrication. The authors also thank Libby Shaw, Charles Settens (MIT), Cheryl Gomes, and Rebecca Ruckdashel (UMass Lowell) for help with the PE fiber and textile characterization. They also gratefully acknowledge useful discussions with Michael Rein, Alexander Stolyarov, and Jason Cox (AFFOA), Mukund Karanjikar (Technology Holding LLC), Val Livada, Joshua Wachman, Leon

Sandler, Karen Golmer, and Christopher Noble (MIT), Taylor Rycroft and Igor Linkov (US Army Engineer Research and Development Center), Maren Cattonar (NERAMCO), Natalie Pomerantz, Molly Richards, and Charlene Mello (CCDC Soldier Center).

Notes

The published version of this article is available at https://www.nature.com/articles/s41893-021-00688-5 with DOI: 10.1038/s41893-021-00688-5

References

1. https://www.grandviewresearch.com/industry-analysis/textile-market (accessed 9/18/20).
2. https://www.wsj.com/articles/the-high-price-of-fast-fashion-11567096637 (accessed 9/187/20).
3. Sweeny, G. It's the Second Dirtiest Thing in the World – And You' re Wearing It, https://www.alternet.org/2015/08/its-second-dirtiest-thing-world-and-youre-wearing-it/.
4. US EPA. Facts and Figures about Materials, Waste and Recycling, https://www.epa.gov/facts-and-figures-aboutmaterials- waste-and-recycling/textiles-material-specific-data (accessed 9/18/20).
5. *A New Textiles Economy: Redesigning Fashion's Future (Ellen MacArthur Foundation, 2017)*.
6. The price of fast fashion. *Nat. Clim. Chang.* **8,** 1 (2018).
7. https://www.un.org/sustainabledevelopment/ (accessed 9/18/20).
8. Boriskina, S. V. An ode to polyethylene. *MRS Energy Sustain.* **6,** E14 (2019).
9. Grigore, M. Methods of recycling, properties and applications of recycled thermoplastic polymers. *Recycling* **2,** 24 (2017).
10. Ragaert, K., Delva, L. & Van Geem, K. Mechanical and chemical recycling of solid plastic waste. *Waste Manag.* **69,** 24–58 (2017).
11. Zhang, Z., Gora-Marek, K., Watson, J. S., Tian, J., Ryder, M. R., Tarach, K. A., López-Pérez, L., Martínez-Triguero, J. & Melián-Cabrera, I. Recovering waste plastics using shape-selective nano-scale reactors as catalysts. *Nat. Sustain.* **2,** 39–42 (2019).
12. Tong, J. K., Huang, X., Boriskina, S. V., Loomis, J., Xu, Y. & Chen, G. Infrared-transparent visible-opaque fabrics for wearable personal thermal management. *ACS Photonics* **2,** 769–778 (2015).
13. Hsu, P.-C., Song, A. Y., Catrysse, P. B., Liu, C., Peng, Y., Xie, J., Fan, S. & Cui, Y. Radiative human body cooling by nanoporous polyethylene textile. *Science (80-.).* **353,** 1019–1023 (2016).
14. Boriskina, S. V. Nanoporous fabrics could keep you cool. *Science (80-.).* **353,** 986–987 (2016).
15. Peng, Y., Chen, J., Song, A. Y., Catrysse, P. B., Hsu, P.-C., Cai, L., Liu, B., Zhu, Y., Zhou, G., Wu, D. S., Lee, H. R., Fan, S. & Cui, Y. Nanoporous polyethylene microfibres for large-scale radiative cooling fabric. *Nat. Sustain.* **1,** 105–112 (2018).
16. Boriskina, S. V, Zandavi, H., Song, B., Huang, Y. & Chen, G. Heat is the new light. *Opt. Photonics News* **28,** 26–33 (2017).
17. Shirvanimoghaddam, K., Motamed, B., Ramakrishna, S. & Naebe, M. Death by waste: Fashion and textile circular economy case. *Sci. Total Environ.* **718,** 137317 (2020).
18. *Fashion Industry Charter for Climate Action*.

19. *Circular Fashion - A New Textiles Economy: Redesigning fashion's future*. (2017).
20. Higg Materials Sustainability Index - https://msi.higg.org/.
21. http://plasticoverde.braskem.com.br/site.aspx/Im-greenTM-Polyethylene.
22. Muthu, S. S., Li, Y., Hu, J. Y. & Mok, P. Y. Recyclability Potential Index (RPI): The concept and quantification of RPI for textile fibres. *Ecol. Indic.* **18,** 58–62 (2012).
23. Allwood, J. M., Laursen, S. E., Rodríguez, C. M. de & Bocken, N. M. P. *Well dressed? The present and future sustainability of clothing and textiles in the United Kingdom*. (2006). doi:ISBN 1-902546-52-0
24. van der Velden, N. M., Kuusk, K. & Köhler, A. R. Life cycle assessment and eco-design of smart textiles: The importance of material selection demonstrated through e-textile product redesign. *Mater. Des.* **84,** 313–324 (2015).
25. Steinberger, J. K., Friot, D., Jolliet, O. & Erkman, S. A spatially explicit life cycle inventory of the global textile chain. *Int. J. Life Cycle Assess.* **14,** 443–455 (2009).
26. Shimel, M., Gouzman, I., Grossman, E., Barkay, Z., Katz, S., Bolker, A., Eliaz, N. & Verker, R. Enhancement of wetting and mechanical properties of UHMWPE-based composites through alumina atomic layer deposition. *Adv. Mater. Interfaces* **5,** 1–9 (2018).
27. Yousif, E. & Haddad, R. Photodegradation and photostabilization of polymers, especially polystyrene: review. *Springerplus* **2,** 398 (2013).
28. Hawkins, W. L. *Polymer Degradation and Stabilization*. **8,** (Springer Berlin Heidelberg, 1984).
29. Abusrafa, A. E., Habib, S., Krupa, I., Ouederni, M. & Popelka, A. Modification of polyethylene by RF plasma in different/mixture gases. *Coatings* **9,** 145 (2019).
30. Eisenreich, N. & Rohe, T. in *Encycl. Anal. Chem.* (John Wiley & Sons, Ltd, 2006). doi:10.1002/9780470027318.a2011
31. Princen, H. M. Capillary phenomena in assemblies of parallel cylinders. II. Capillary rise in systems with more than two cylinders. *J. Colloid Interface Sci.* **30,** 359–371 (1969).
32. Zhang, J. & Han, Y. Shape-gradient composite surfaces: Water droplets move uphill. *Langmuir* **23,** 6136–6141 (2007).
33. Wallenberger, F. T. The effect of absorbed water on the properties of cotton and fibers from hydrophilic polyester block copolymers. *Text. Res. J.* **48,** 577–581 (1978).
34. *Polyolefin Fibres: Structure, Properties and Industrial Applications*. (Woodhead Publishing, 2017).
35. Lozano, L. M., Hong, S., Huang, Y., Zandavi, H., El Aoud, Y. A., Tsurimaki, Y., Zhou, J., Xu, Y., Osgood, R. M., Chen, G. & Boriskina, S. V. Optical engineering of polymer materials and composites for simultaneous color and thermal management. *Opt. Mater. Express* **9,** 1990 (2019).
36. Cai, L., Peng, Y., Xu, J., Zhou, C., Zhou, C., Wu, P., Lin, D., Fan, S. & Cui, Y. Temperature regulation in colored infrared-transparent polyethylene textiles. *Joule* **3,** 1478–1486 (2019).
37. Geyer, R., Jambeck, J. R. & Law, K. L. Production, use, and fate of all plastics ever made. *Sci. Adv.* **3,** e1700782 (2017).
38. Bisinella, V., Albizzati, P. F., Astrup, T. F. & Damgaard, A. *Life Cycle Assessment of grocery carrier bags*. (2018).
39. Ni, G. W., Zandavi, S. H., Javid, S. M., Boriskina, S. V., Cooper, T. A. & Chen, G. A salt-rejecting floating solar still for low-cost desalination. *Energy Environ. Sci.* **11,** 1510–1519 (2018).

40. Alberghini, M., Morciano, M., Fasano, M., Bertiglia, F., Fernicola, V., Asinari, P. & Chiavazzo, E. Multistage and passive cooling process driven by salinity difference. *Sci. Adv.* **6,** eaax5015 (2020).
41. Lal Basediya, A., Samuel, D. V. K. & Beera, V. Evaporative cooling system for storage of fruits and vegetables - A review. *J. Food Sci. Technol.* **50,** 429–442 (2013).
42. McLain, V. C. Final report on the safety assessment of Polyethylene. *Int. J. Toxicol.* **26,** 115–127 (2007).
43. Suhardi, V. J., Bichara, D. A., Kwok, S. J. J., Freiberg, A. A., Rubash, H., Malchau, H., Yun, S. H., Muratoglu, O. K. & Oral, E. A fully functional drug-eluting joint implant. *Nat. Biomed. Eng.* **1,** 1–11 (2017).
44. Halden, R. U. Plastics and Health Risks. *Annu. Rev. Public Health* **31,** 179–194 (2010).
45. GORE-TEX. LCA journey continues: Gore offers solution dyed and recycled textiles. (2017). at <https://www.gore.com/news-events/press-release/fabrics-offers-solution-dyed-and-recycled-textiles>
46. Terinte, N., Manda, B. M. K., Taylor, J., Schuster, K. C. & Patel, M. K. Environmental assessment of coloured fabrics and opportunities for value creation: Spin-dyeing versus conventional dyeing of modal fabrics. *J. Clean. Prod.* **72,** 127–138 (2014).
47. Greener textile dyeing. *C&EN Glob. Enterp.* **96,** 28–33 (2018).
48. Carroll, B. J. Accurate measurement of contact angle, phase contact areas, drop volume, and Laplace excess pressure in drop-on-fibre systems. *J. Colloid Interface Sci.* **57,** 488–495 (1976).
49. Kralchevsky, P. A., Paunov, V. N., Ivanov, I. B. & Nagayama, K. Capillary meniscus interaction between colloidal particles attached to a liquid-fluid interface. *J. Colloid Interface Sci.* **151,** 79–94 (1992).
50. Masoodi, R. & Pillai, K. M. *Wicking in Porous Materials : Traditional and Modern Modeling Approaches*. (CRC Press Taylor & Francis, 2012). doi:10.1201/b12972
51. Princen, H. M. Capillary phenomena in assemblies of parallel cylinders. I. Capillary rise between two cylinders. *J. Colloid Interface Sci.* (1969). doi:10.1016/0021-9797(69)90379-8
52. Core Team, R. *R: A language and environment for statistical computing. R Foundation for Statistical Computing*. (2019).